Please do not adjust margins

Journal Name

ARTICLE

Novel solid forms of lonidamine: crystal structures and physicochemical properties

Received 00th January 20xx,
Accepted 00th January 20xx

DOI: 10.1039/x0xx00000x

www.rsc.org/

Lucy K. Mapp,[ab] Simon J. Coles[b] and Srinivasulu Aitipamula*[a]

Lonidamine finds potential applications in cancer treatments, and its current marketed solid form, the sodium salt, displays poor solubility. The presence of a single carboxylic acid group make it an ideal target for co-crystal design as design strategies involving carboxylic acid groups are well-established. CSD statistics combined with known hydrogen bonding preferences allowed suitable co-former selection which resulted in nine new multicomponent crystals with pharmaceutically acceptable co-formers. These included co-crystals, salts and some hybrid (co-crystal salt) structures. All the solid forms were characterized by X-ray diffraction techniques with subsequent measurement of physicochemical properties, such as stability, solubility, and dissolution rate. It was found that the co-formers were able to modulate the properties of ~~L~~lonidamine.

Formatted: English (United Kingdom)

Introduction

Co-crystallisation has been widely known in recent years as a favourable approach to generate new and alternative solid forms of compounds.[1] Co-crystals can be described as molecular complexes comprising two (or more) different molecules in a stoichiometric ratio[2,3]. They must be solids under ambient conditions, occur in their neutral form,[4] and be held in place through directional, freely reversible, non-covalent interactions.[5,6] Solvent and/or water molecules may be present as an additional molecule giving rise to co-crystal solvates and/or hydrates. Recently, de Gelder et al[7] proposed a classification system for all multicomponent crystal systems consisting of seven classes arising from three main groups. This allows pure co-crystals to be distinguished from salts, solvates, and hybrid structures (which bridge the, for example, co-crystal-salt boundary). It also creates a separation from host-guest inclusion complexes and other such materials. Co-crystals have found prominence through their effectiveness in modifying and fine-tuning physicochemical properties.[6,8] This is achieved through appropriate co-former selection, especially in the pharmaceutical field. Pharmaceutical co-crystals[8-11] contain an active pharmaceutical ingredient (API) and pharmaceutically acceptable co-former molecules: U.S. Food and Drug Administration (FDA) approved GRAS (generally recognised as safe)[12] compounds or those listed on EAFUS (everything added to foodstuffs in the United States).[13] Co-crystallisation offers potential advantages, having been proved effective in addressing issues such as poor solubility[14-16] as well as modifying properties such as stability,[17,18,~~19~~] bioavailabilty[16,~~20~~~~19~~] and mechanical[2~~19~~] properties.

Lonidamine (1-(2,4-dichlorobenzyl)-1H-indazole-3-carboxylic acid, LON, Figure 1) is a hexokinase inhibitor[2~~1~~] causing glycolysis enzyme inactivation. In this way it can help induce apoptosis as well as causing cell death through interference in angiogenesis.[2~~3~~] These qualities demonstrate that LON is a good candidate for cancer treatment and it has been formulated as such in Italy, as ~~Doridamine~~doridamine.[2~~3~~] Encouraging results have been reported from a number of studies utilising LON for cancer treatment either on its own[2~~4~~] or as a combination treatment.[2~~5~~ ~~2~~~~8~~] There are also uses for the drug in neurodegenerative and neuromuscular diseases, obesity and diabetes.[2~~5~~,2~~8~~,30~~29~~] Thus, there is reasonable evidence that this compound is of therapeutic interest and the formulation of alternate solid forms may be of interest. In particular, as both LON and its sodium salt exhibit very low solubility[3~~0~~] creating a hindrance in drug formulation and delivery.

The current study was aimed at exploring novel solid forms of LON with an objective to modify its physicochemical properties. A solid form screening, incorporating structural knowledge from the Cambridge Structural Database (CSD), resulted in nine different pharmaceutically acceptable solids which include co-crystals, salts and hybrids of both. We herein report crystal structures and physicochemical properties of the novel pharmaceutically acceptable solid forms of LON.

[a] Crystallization and Particle Sciences, Institute of Chemical and Engineering Sciences, A*STAR (Agency for Science, Technology and Research), 1 Pesek Road, Jurong Island, Singapore, 627833.
E-mail: srinivasulu_aitipamula@ices.a-star.edu.sg
[b] Chemistry, Faculty of Natural and Environmental Sciences, University of Southampton, University Road, Southampton, SO17 1BJ, UK.

† Electronic Supplementary Information (ESI) available: polymorph determination and analysis of bulk material, co-former list, PXRD analysis (grinding and stability tests), crystal structure parameters and hydrogen bond tables, pK_a analysis, additional thermal properties data. See DOI: 10.1039/x0xx00000x

Please do not adjust margins

Please do not adjust margins

~~Results and discussion~~

Lonidamine polymorphs. Three polymorphic forms of LON are known, two of which (α and β) were reported by Benetollo et al[31,0] with an in-depth structural analysis and structure-activity relationship of the β-form. More recently, a patent by Xinmin et al[32,1] described three forms which can be identified as the two from Benetollo's work with a third, new form. Through powder X-ray diffraction (PXRD) and differential scanning calorimetry (DSC) data, the work in these two reports can be correlated: α- and β- correspond respectively to forms I and II in the patent, with the third form being assumed as a new γ-phase (see ESI, section 1).

Benetollo et al have reported the crystal structure of the β-form, along with reference to an α-form with some physical properties measurements. The crystal structure of the latter is reported herein. Both the polymorphs form acid···acid dimers which are connected through C-H···O interactions into chains (Figure 1). It is noted that the bulk LON material used for all experiments in our study is a mixture of both α- and β-polymorphs, however with a greater proportion of β (see ESI, section 2). The two polymorphs can be produced separately through careful solvent selection, (see ESI, section 3) although formation of the pure α-form is more challenging than the β-form using solvent based crystallisation methods.

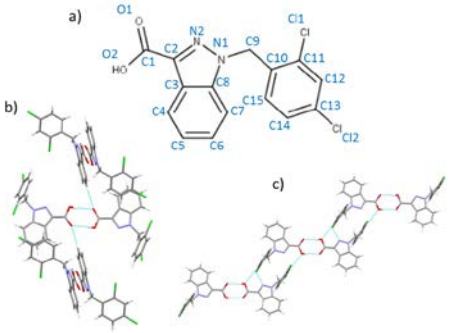

Figure 1. a) Chemical diagram of LON with labelling scheme employed for all structures herein, and main interaction pattern present in b) α-LON and c) β-LON.

Results and discussion

Co-former selection. Crystal engineering strategies are predominantly used for co-former selection, identifying commonly occurring supramolecular synthon motifs[33,2] based upon robust intermolecular interactions identified from existing structures. Visual inspection and structural analysis of LON polymorphs indicates that the potential for strong intermolecular interactions arises predominantly from the carboxylic acid group.

Utilising the tools available from the Cambridge Crystallographic Data Centre (CCDC), implemented in Mercury[34,3-36,5] and Conquest,[34,3] it was found that the most preferential interactions of the carboxylic acid group include those to amides, primary amines (-NH_2), aromatic nitrogen atoms (for example pyridines) and hydroxyls. In structures which contain these functionalities, the intermolecular interactions between carboxylic acid and the respective functional groups occur at a propensity of 77.2 %, 67.2 %, 63.8 % and 35.3 % (any OH). Hydroxyl groups can be further divided: alcoholic OH groups are highly favoured (66 %) with general aromatic and aliphatic OH groups displaying propensities around 50%. The hierarchy of interactions for a carboxylic acid is therefore amides > primary amines (-NH_2) > aromatic nitrogen atoms > hydroxyls. Dimer interactions are also highly favoured, with 87.3 % of structures containing two carboxylic acid groups forming a dimer, and a 46.5 % frequency in the acid···amide equivalent. See ESI, section 4 for a detailed breakdown of this analysis.

The other functional group present in LON is the indazole, which, according to CSD statistics, can interact favourably with C-H groups, hydroxyls, primary amines, amides and T3NH_1 (one hydrogen atom, total three bonded atoms to N) groups. Interactions involving an indazole group occur in fewer structures (smaller result sets) and with lower propensities for interactions with common hydrogen bond functionalities. This indicates it is a much weaker functionality than the carboxylic acid in the hierarchy of interactions and synthons. A carboxylic acid would preferentially form interactions in a molecule containing both a carboxylic acid and indazole functionality; however both may form an interaction depending on the nature of the co-former and number of available functional groups. This is in accordance with Etter's rules of hydrogen bonding, whereby the best proton donors and acceptors, after intramolecular interactions are considered, will form interactions to one another.[37,6]

Solid form screening. Potential co-formers for LON were primarily selected based upon the findings from the CSD analysis. A total of 87 structurally diverse compounds (see ESI, section 5) were chosen for experimental screening by solid-state grinding (both solvent assisted and dry grinding). This diversity ensured that potential intermolecular interactions to the API were not restricted to just those identified. However, the selection did include a large number of molecules containing these functionalities, as these were the most likely to generate a new form.

Samples generated through grinding were analysed using PXRD and compared to reference patterns (ESI, section 6). Subsequently, solution crystallisation experiments were conducted to produce single crystals suitable for diffraction studies. Solid form screening with LON resulted in a total of nine different solids with seven pharmaceutically acceptable co-formers (Figure 2): benzamide (BENZ), haloperidol (HALO), imidazole (IMID), isonicotinamide (ISO), melamine (MEL), nicotinamide (NICO), and piperazine (PIPE). A number of multi-component solids were also formed with non-pharmaceutically acceptable co-formers (see ESI, Section 6.2). Cell parameters, structural information and hydrogen bonding parameters for all the novel forms are detailed in the ESI, section 7.

This journal is © The Royal Society of Chemistry 20xx

Please do not adjust margins

Please do not adjust margins

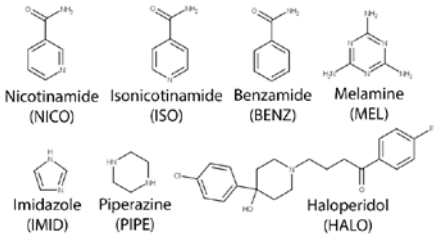

Figure 2. Chemical diagrams of the pharmaceutically acceptable co-formers that formed novel solids with LON.

Crystal Structure Analyses.

LON-BENZ (1:1) co-crystal. The primary hydrogen bonding present in the 1:1 LON-BENZ co-crystal is an acid···amide dimer (D···A distances 2.55 Å and 2.88 Å, D–H···A angles 172° and 169° for O-H···O and N-H···O respectively). An additional hydrogen bond occurs from the NH_2 in a bifurcated pattern interacting with both the indazole nitrogen atom (N-H···N) and acid hydroxyl (N-H···O) of a second LON molecule. This results in a 4-membered supramolecular unit, similar to that seen in α-LON. These assemble into zig-zag chains with a head-to-head arrangement of adjacent chains (Figure 3).

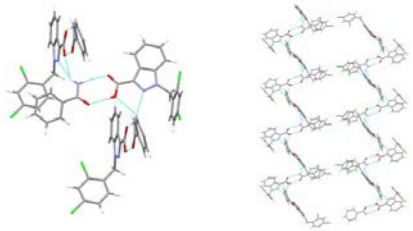

Figure 3. Left, primary hydrogen bond motif in the 1:1 LON-BENZ co-crystal and right, zig-zag chains.

LON-NICO (1:1) co-crystal. Nicotinamide also forms a 1:1 co-crystal with LON and features an acid···amide dimer as the primary hydrogen bonding interaction (2.53 Å and 2.96 Å, 169° and 168° for O-H···O and N-H···O respectively). A further hydrogen bond (N-H···O, 2.85 Å, 119°) forms from the amide in NICO to the LON carbonyl in a second dimer pair. This results in tetrameric supramolecular units (Figure 4) which occur in two planes arranged almost perpendicular to one another (88°), and stack into layers in these two orientations.

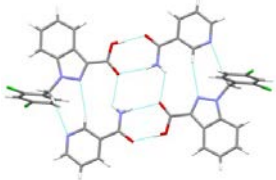

Figure 4. Tetramer arrangement of dimers in the LON-NICO 1:1 co-crystal.

LON-ISO (1:1) co-crystal. The 1:1 LON-ISO co-crystal also features a tetrameric motif (Figure 5), however, this is formed through an acid···pyridine (2.64 Å, 176°) and amide (N-H)···carbonyl (2.97 Å, 175°) hydrogen bonds. As seen for LON-NICO, the tetrameric motif is not planar, as the co-former molecules sit slightly above and below the plane of the carboxylic acids with a tilted orientation. N-H···O hydrogen bonds and C-H···O interactions connect the tetramers, which occur with two general orientations, and stack in chains of the tetrameric units down the *b*-axis.

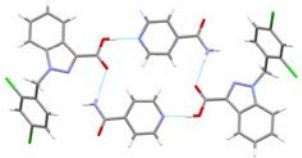

Figure 5. Tetramer arrangement of LON and ISO molecules in the 1:1 co-crystal structure.

LON-MEL (1:1) salt. Melamine forms a 1:1 molecular adduct with LON, however, proton transfer occurs generating a salt form rather than a co-crystal. The crystal structure of the salt features a bifurcated hydrogen bond from the protonated pyridine N and adjacent amino group to the LON carboxylate O1 (2.65 Å and 3.01 Å, 157° and 138° respectively). A second hydrogen bond occurs from the same amino group via the other proton to a second LON, forming an N-H···O hydrogen bond to O2 of the carboxylate (2.99 Å, 173°) also with a weak interaction to O1. The other amino group adjacent to the ring N^+-H forms an N^+-H···N hydrogen bond (3.01 Å, 171°) to the indazole of LON. The third amino group of MEL forms a co-former···co-former dimer via two N-H···N hydrogen bonds (2.91 Å, 175°). These interactions create a ladder network containing central MEL pairs and peripheral LON molecules (Figure 6) with face-to-face π-π stacking between ladders, all of which are parallel.

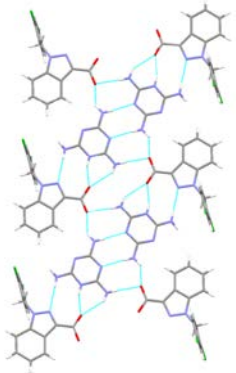

Figure 6. Ladder arrangement in the 1:1 LON-MEL salt.

LON-PIPE (2:1) salt. LON-PIPE forms a 2:1 salt containing charge assisted N^+-H···carboxylate hydrogen bonds (2.69 Å, 2.64 Å, 2.69 Å and 2.76 Å, 164°, 159°, 172° and 163°) from

Please do not adjust margins

Please do not adjust margins

each LON molecule to the symmetry independent half molecules of PIPE. These produce a ladder network, in the *a*-direction, and also contain central PIPE molecules with a peripheral LON backbone (similar to LON-MEL, Figure 6). The PIPE molecules form an ABAB type layered stacking arrangement (Figure 7) with alternating orientations. 'A' piperazine molecules form a single N^+-H···carboxylate and a similar, bifurcated, hydrogen bond at either end of the piperazine molecule. The bifurcated hydrogen bond occurs to both atoms of a single carboxylate on one LON moiety. 'B' piperazine molecules also form a single N^+-H···carboxylate and a bifurcated N-H hydrogen bond at either end of the molecule, however the latter occurs to one carboxylate oxygen and one indazole ring nitrogen.

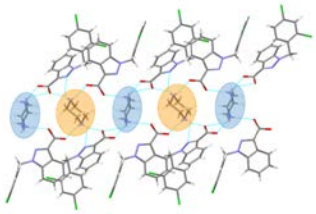

Figure 7. Ladder network in the crystal structure of 2:1 LON-PIPE salt with alternating orientation of central PIPE molecules giving an ABAB type packing. 'A' PIPE molecules depicted in blue, 'B' in orange.

LON-IMID. Three different structures were obtained with LON and IMID: a 1:1:0.5 ethyl acetate salt, a 1:1 salt and a 2:1 co-crystal salt (hybrid structure). For detailed information on disorder and crystal structure parameters see ESI, section 7.3.2.

The 1:1 salt solvate contains 6 molecules of both LON and IMID in the asymmetric unit, and three ethyl acetate molecules. LON-IMID units assemble via two bifurcated hydrogen bonds involving the IMID N-H. One consists of two N-H···$O_{(carboxylate)}$ interactions (eg 2.63 Å, 167° and 3.43 Å, 125°), the other comprising charge assisted hydrogen bonds of the nature N^+-H···$O_{(carboxylate)}$ and one N^+-H···$N_{(indazole)}$ (2.69 Å, 153° and 3.08 Å, 125° respectively). These hydrogen bonded units extend in zig-zag chains which contain an ABAB type pattern of IMID molecules (Figure 8, left). All LON chloro-substituted rings are situated above the chain and display alternating orientations complementary to the ABAB motif. The chains form parallel stacked sheets extending into layers. The packing results in voids along the *b*-axis in which the solvent molecules are located.

The 1:1 LON-IMID salt contains two molecules of each entity in the asymmetric unit with complete proton transfer occurring between one pair and partial transfer between the second. A similar chain motif to that observed in the 1:1:0.5 salt solvate was also observed in the 1:1 salt (Figure 8, middle). The layers, however, are arranged in an ABBAABBA pattern, considered in terms of the co-former molecules. The 'A' layer consists of a protonated IMID which interacts with a self-assembled dimer of partially protonated LON units (bifurcated N^+-H···O to hydroxyl (2.67 Å, 170°) and carbonyl oxygen atoms (2.79 Å, 141°) and an N-H···$O^-_{(carboxylate)}$ hydrogen bond to both oxygen atoms of a third, deprotonated, LON (N-H···O^-, 2.56 Å, 166° and 3.40 Å, 125°). The 'B' IMID molecule is partially protonated (occupancy 0.5, shared with a second 'B' IMID) and forms an IMID dimer via N^+-H···N hydrogen bonds over an inversion centre. This forms a bifurcated hydrogen bond to the deprotonated LON mentioned above via N-H···$O^-_{(carboxylate)}$ (2.76 Å, 160°) and N-H···$N_{(indazole)}$ (3.12 Å, 122°). Adjacent chains stack into layers containing face-to-face orientated LON chloro-substituted rings.

The final IMID salt has a 2:1 ratio and contains units of the same stoichiometry containing N-H···$O_{(carbonyl)}$ hydrogen bonds (2.69 Å, 159° and 2.76 Å, 169°). Both LON molecules possess a half occupied hydrogen atom whilst IMID is fully protonated, thus making a charge-balanced unit. In a similar way to the 1:1 salt, LON dimers form via O-H···$O_{(carboxylate)}$ hydrogen bonds (2.51 Å, 173°) connecting the 2:1 units along the *c*-axis in chains (Figure 8, right). The chains stack to form parallel layers generating the 3D lattice. There are solvent accessible voids present (110 $Å^3$) which could contain / uptake solvent or water molecules however residual density analysis indicates no electron density present.

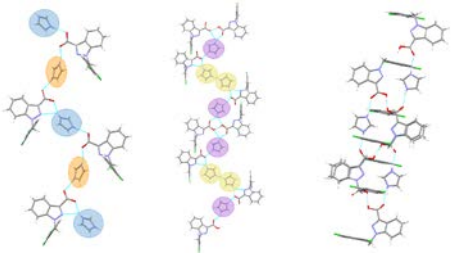

Figure 8. Main hydrogen bonds present in the LON-IMID structures. Left, LON-IMID 1:1 salt solvate ladders with ABAB pattern (blue 'A' and orange 'B', solvent excluded for clarity), middle, LON-IMID 1:1 ladders with ABBA pattern (purple 'A' and yellow 'B') and right, 2:1 structure showing LON dimer interactions between 2:1 units.

LON-HALO (1:1) hydrate. LON-HALO forms a 1:1 trihydrate salt containing a primary N^+-H···O^- hydrogen bond (2.72 Å, 172°). Additional hydrogen bonds involving the water molecules extend the network via the same carboxylate oxygen partaking in the charge assisted LON-HALO hydrogen bond (O-H···$O_{(carboxylate)}$), as well as through O-H···O hydrogen bonds between water molecules. A tetrameric supramolecular unit, consisting of two LON molecules (carboxylate end) connected via two water molecules, forms around an inversion centre and is surrounded by two HALO molecules (Figure 9). These HALO molecules are situated one each above and below the tetramer plane and form N^+-H···O^- hydrogen bonds.

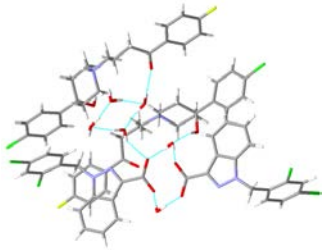

This journal is © The Royal Society of Chemistry 20xx

Please do not adjust margins

Please do not adjust margins

Figure 9. Main hydrogen bonds present in the 1:1 LON-HALO trihydrate salt, consisting of two tetramers: one containing two LON molecules and two water molecules and the second a self-assembling tetramer of four water molecules. These are linked via a water···carboxylate hydrogen bond, and extend into a lattice through various tetramer···HALO hydrogen bonds.

Proton Transfer and pK_a. LON forms a wide range of multi-component solids: co-crystals (no proton transfer), salts (complete proton transfer), and co-crystal salts (hybrid structures containing partial proton transfer). The rule of three[38,39] has been well established as a tool to predict co-crystal or salt formation: If ΔpK_a (pK_a (protonated base) − pK_a (acid)) of the acid and base is greater than 3 proton transfer will occur and a salt results, while if < 0 no proton transfer will take place and a co-crystal will be produced. The intermediate range between 0 and 3 is harder to categorise,[40,39,42,1] making systems with ΔpK_a values in this range difficult to predict.

For all the systems reported herein, pK_a values were predicted using the physiochemical properties calculator plugin[43] as implemented in MarvinSketch[44] and the prediction methodology is described in ESI, section 8. The rule of three works in just over half of the solids reported in this study, however some discrepancies are present, especially for those with ΔpK_a values between 0 and 3. There were also combinations which produced multiple experimental structures which are also hard to predict. As expected, all structures exhibiting a degree of partial proton transfer lie within the 0-3 range. As reported by Park et al,[45] solution pK_a values are not wholly reliable when applied to the solid state. If the cut off values are set more leniently, e.g. the generally accepted ΔpK_a differences of above 2 or 3 for salt formation and less than 0 or 1 for co-crystal production, all predictions reported herein can be considered correct.

Thermal Analysis. DSC curves are shown in Figure 10 and the melting points of the new materials are compared with reference data in Table 1. Of the three solid forms of LON-IMID, only the 1:1 salt solvate (LON-IMID.EtOAc) was analysed by DSC. All co-crystals (LON-NICO, LON-ISO and LON-BENZ) showed a lower melting point (in accordance with the lower melting point of the co-formers)[46,47,76] whilst all salts, except the LON-IMID salt solvate, showed a higher melting point compared to that of LON. This can be ascribed to the presence of strong charge assisted hydrogen bonds in the salt structures. LON-MEL showed the highest melting point among all the solid forms reported herein. The LON-IMID.EtOAc salt solvate showed the lowest melting point of all materials, due to the low co-former melting point and concomitant desolvation and melting. The LON-HALO trihydrate shows a broad endotherm between 60-80 °C and jagged multiple endotherms between 105-125 °C. Water loss from hydrate crystals can be a complex event, dependent upon the location of the water molecule in the crystal lattice and the number of hydrogen bonds that it forms with the parent molecules. These occurrences in the endotherm can be attributed to such water loss events. Water loss (and solvent loss, as in LON-IMID.EtOAc) causes lattice breakdown due to hydrogen bonds being broken; the network is disrupted and results in the sample melting. The behaviour in both samples was further investigated by hot-stage microscopy (ESI, section 10). This showed that water loss and melting occur simultaneously in LON-HALO.$3H_2O$ over a broad temperature range (75-125 °C). In LON-IMID.EtOAc solvent loss and melting also occur concomitantly, but over a narrower range (81-88 °C). A broad endotherm following the melt (as seen in LON-HALO.$3H_2O$ around 275 °C, LON-BENZ around 215 °C and to some extent following the melt in LON-PIPE and LON-MEL) is most likely due to decomposition of the melt. HSM investigations of LON-HALO.$2H_2O$ and LON-IMID.EtOAc confirmed the nature of this event.

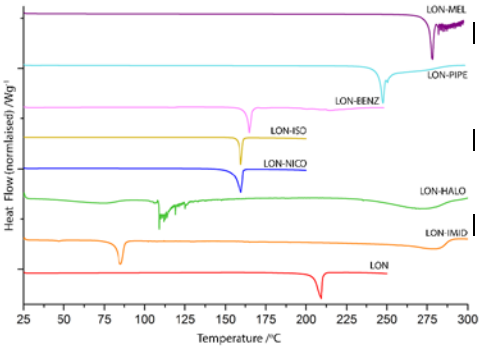

Figure 10. DSC plots for LON and the new co-crystals and salts (showing LON-IMID 1:1 salt solvate only). Note two samples are solvates/hydrate: LON-HALO.$3H_2O$ and LON-IMID.EtOAc.

Table 1. Experimental melting points for LON, its co-crystals and salts compared with co-former reference melting points.

Sample	Melting Point (T_{onset})/°C	Co-former Melting Point /°C
LON	204.6	
LON-BENZ	163.3	127-130
LON-HALO (trihydrate)	104.7#	148-152
LON-IMID	81.1##	88-91
LON-ISO	158.4	156
LON-MEL	276.7	345-350
LON-NICO	155.0	128-130
LON-PIPE	242.1	109-113

#LON-HALO displays a number of events which can be described as water loss (60-80 °C), melting (105-125 °C) and decomposition 233 °C. ##LON-IMID also displays a decomposition event from 240 °C, with the event at 81.1 °C consisting of desolvation and concomitant melting.

Stability of Pharmaceutically Acceptable Co-Crystals and Salts. Dynamic Vapour Sorption (DVS) measures water (or solvent) uptake of a powder with an increasing partial pressure over a given time period. Uptake is determined through sample mass change. Figure 11 shows the sorption and desorption profiles for the new materials along with LON. Two samples show a mass change greater than 1 %, ~~the~~ LON-IMD.EtOAc ~~salt solvate~~ 1.9 % and ~~the~~ LON-HALO.$3H_2O$ ~~salt trihydrate~~ 2.6 %. This suggests that the water uptake is beyond

Please do not adjust margins

surface adsorption. Interestingly, these two salts contain solvent/water molecules in their crystal lattices. Further analysis of the crystal structures indicates the presence of voids (56.48 Å³ LON-IMID.EtOAc and 44.63 Å³ LON-HALO.$2H_2O$), each capable of accommodating a water molecule, which explains the observed water uptake.

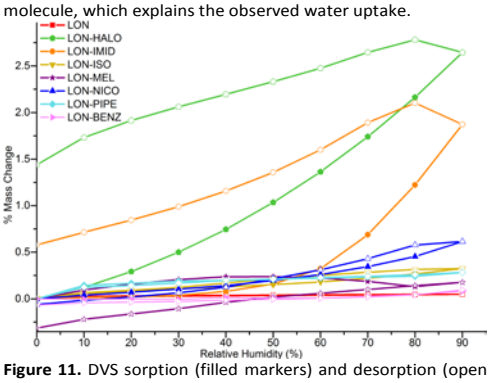

Figure 11. DVS sorption (filled markers) and desorption (open markers) plots for LON and new co-crystal and salt materials. Note two samples are solvates/hydrate: LON-HALO.$3H_2O$ and LON-IMID.EtOAc.

Stability of the pharmaceutically acceptable solids was tested under slurry and accelerated test conditions (40 °C / 75 % relative humidity). For slurry conditions, excess powders of the solids were stirred in 1 % Tween 80® aqueous media at room temperature for 24 h. After this period the solids were filtered, dried and analysed by PXRD (see ESI, section 9). Aliquots of the slurry solution were appropriately diluted and analysed for solubility estimation by high-performance liquid chromatography (HPLC). It can be seen from PXRD analysis that the LON-NICO and LON-ISO co-crystals, as well as the IMID salt solvate, demonstrated poor stability. Dissociation into component parts was apparent and evidenced by the appearance of parent LON peaks (predominantly β-LON with a degree of both polymorphs identified in LON-NICO) and some co-former reference peaks in the PXRD analysis. The poor stability of these co-crystals could be due to weaker hydrogen bonds compared to the charge-assisted hydrogen bonds in salts.

Under accelerated storage conditions all samples appear stable with the exception of the imidazole salt solvate. The poor stability of LON-IMID.EtOAc salt solvate could be attributed to the presence of ethyl acetate solvent molecules in the crystal lattice. Solvent molecules occupy the large voids with no hydrogen bonding, hence solvent removal occurs readily and leads to dissociation of the molecular salt into its individual components. Stability studies suggest that the anhydrous/non-solvated salts showed the highest stability among the solid forms reported herein.

Solubility and Dissolution Rate. To optimise drug performance, maximum and equilibrium concentrations (kinetic and thermodynamic solubility respectively) are essential in order to understand the substances' behaviour and drug release. As shown in stability tests (ESI, section 9), the two co-crystals with ISO and NICO, and ~~the~~ LON-IMID.EtOAc salt solvate are unstable under slurry conditions. Additionally the LON-IMID salt solvate showed water uptake in DVS (Figure 11) and a low melting point, reinforcing the poor stability. For the stable samples, the concentration of filtered aliquots (obtained from slurry experiments) represents the true solubility of the sample as they remain intact in these conditions. For the unstable materials, apparent solubility[48,49] was calculated from the linear portions of the respective dissolution curves.

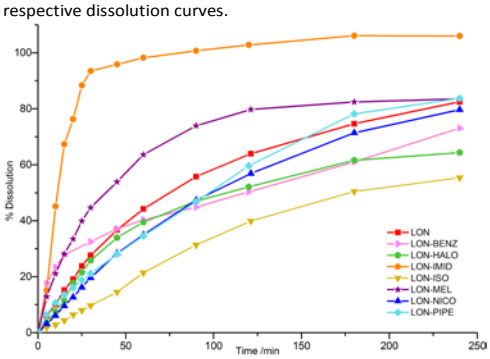

Figure 12. Dissolution rate profile for LON and the new salts and co-crystals over 240 minute experiment in 1% Tween 80® aqueous media. Note two samples are solvates/hydrate: LON-HALO.$3H_2O$ and LON-IMID.EtOAc.

Table 2. Dissolution and Solubility data.

Sample	% Dissolution in 30 mins	Solubility /mgmL^{-1}	Ratio to API
LON	27.7	0.115	1
LON-BENZ	32.5	0.130	1.13
LON-HALO	25.8	0.175	1.52
LON-IMID (solvate)	93.5	0.511 [a]	4.45
LON-ISO	9.7	0.055 [a]	0.48
LON-MEL	44.7	0.041	0.36
LON-NICO	19.7	0.093[a]	0.81
LON-PIPE	21.1	2.987	26.0

[a]Apparent solubility

The solubility of the new materials is compared with that of LON in Table 2. The highest solubility is observed for PIPE, followed by IMID and HALO (all salts). Two of the three co-crystals result in lower solubility, whilst one (LON-BENZ) shows a slightly increased solubility when compared to the parent material. LON-MEL is the only salt material which produced a lower solubility, and could be due to the lower aqueous solubility of the co-former (3.24 mg mL^{-1}).

Increased initial dissolution rate is appealing for a drug molecule as a fast dissolution results in a quicker release of the drug product from the tablet/formulation. As shown in Figure 12, an improvement is seen in the salts with melamine and imidazole and the co-crystal with benzamide. As discussed, LON-IMID is unstable and readily dissociates, resulting in the increased dissolution rate observed. Both LON-NICO and LON-ISO show a degree of dissociation under slurry conditions (extended time period). Neither sample shows an increase in dissolution rate or solubility (as might be expected for a

This journal is © The Royal Society of Chemistry 20xx

Please do not adjust margins

dissociable co-crystal), which can be attributed to the interactions present in the crystal structures. Both LON-NICO and LON-ISO have more hydrogen bond interactions from LON than either of the LON polymorphs, as well as additional co-former···co-former hydrogen bonds. The increased number, as well as some shorter bonding distances, makes the hydrogen bonding network more difficult to disrupt. Dissolution accordingly proceeds at a slower rate. Due to the extended time period of the slurry experiment dissociation starts to occur for these materials with some conversion to parent API. This causes the lower observed solubility. LON-BENZ displays a similar interaction network to α- and β-LON, with fewer hydrogen bonds and the main dimer interaction having slightly longer bonding interactions. This enables the increased dissolution rate and solubility.

LON-PIPE displays a similar initial dissolution rate to LON, however due to the increased solubility it might be expected that the dissolution rate would also be increased. The initial dissolution rate is dependent on kinetics and may be impeded due to the larger relative proportion of poorly soluble LON present (2:1 ratio). Over extended time periods, towards the end of the dissolution and in the equilibrium solubility determination, thermodynamics will have a greater influence. This is displayed in the LON-PIPE dissolution curve, in which the dissolution rate is increasing at the fastest rate of all samples at the end of the experiment. This would suggest a high solubility, but with a kinetic barrier.

CONCLUSIONS

Nine new pharmaceutically acceptable multicomponent materials have been produced with LON. As expected, the carboxylic acid group of LON forms the primary interactions in all crystal structures, which are varied in their nature. A number of structural similarities can be seen across the set, such as the existence of tetrameric (LON-ISO and LON-NICO), ladder (LON-MEL and LON-PIPE) and ladder-related-chain (LON-IMID) motifs.

When compared to the CSD analysis of interactions for the functional groups of LON, the crystal structures obtained display interactions as might be expected. Two structures featured acid-amide dimers, with a further two (1:1 and 2:1 LON-IMID) containing a dimer formed via a single hydrogen bond with a shared proton (O-H···H-O). Three structures (LON-MEL, LON-ISO and LON-PIPE) display $NH_2\cdots O_{LON}$ interactions, five structures contain $N\text{-}H\cdots O_{LON}$ interactions with one displaying a hydrogen bond from the carboxylic acid to a pyridyl N. $C\text{-}H\cdots O_{LON}$ contacts are also seen in a number of structures, and include CH_2 and aromatic C-H groups. The prevalence of N-H interactions is slightly higher than might be expected, however these include charge assisted hydrogen bonds and are hence favoured due to a stronger electrostatic component. The indazole group partakes in interactions with two general types of functionalities: C-H containing (the most prevalent being aromatic C-H) and N-H containing (the most prevalent functional group being NH_2) groups in approximately equal numbers. The observed intermolecular interactions in the solid forms of LON are consistent with the CSD analyses and hierarchy of interactions.

Physiochemical properties for materials containing pharmaceutically acceptable co-formers were measured and it was found that the co-formers were able to modulate the properties of LON. Both increased and reduced melting points were observed, an equivalent or improved stability compared to LON was recognized in three of the salt materials and one co-crystal. Initial dissolution rates were improved in three materials (LON-IMID, LON-MEL and LON-BENZ) with one also showing an improved solubility (LON-BENZ). This makes LON-BENZ an ideal new form of LON, showing an improvement in several important properties. An increase in solubility was also seen in LON-IMID, however it has been shown to be unstable and dissociates into component materials. LON-MEL exhibits a lower solubility than LON. Two of the other salts (LON-PIPE and LON-HALO) showed an improvement in their solubility however, this was not reflected in the dissolution rate.

EXPERIMENTAL

LON was purchased from Junda Pharmaceuticals Ltd., China whilst all co-formers were purchased from Sigma Aldrich, Singapore, with HALO purchased from TCI chemicals, Singapore. All were used as received without any further purification. Analytical grade solvents were used for the crystallisation experiments and HPLC grade for all mobile phase solutions.

Screening by grinding. 1:1 Stoichiometric ratios of LON and co-former were added to a 10 mL stainless steel grinding jar with 7 mm stainless steel ball and ground for 30 minutes at 20 Hz using a Retsch MixerMill (models MM301 and MM200). Solvent drop grinding had 2 drops of methanol added to the jars prior to the start of grinding. PXRD was used to characterise the materials produced with reference to the starting materials to identify whether changes were present, and hence a new solid form produced.

Single crystal preparation by solution crystallisation. Solvent evaporative methods were used to prepare single crystals of the new materials that were identified as promising from the screening by grinding. These were used in single crystal X-ray diffraction experiments.

α- and β-LON polymorphs: Different polymorphs could be obtained via careful solvent selection. Crystals of β-LON were obtained from methanol, tetrahydrofuran, dimethylsufoxide, dimethylformamide, formic acid and a methanol-acetonitrile mix.

Crystals of α-LON were obtained in a number of solution co-crystallisation trials in which a co-crystal was not successfully formed, and predominantly using ethyl acetate as the solvent. The crystal used for structure solution was obtained from an ethyl acetate-acetonitrile solvent mix, heated to 50 °C to dissolve commercial LON and then left at ambient conditions. Small colourless crystals were formed after a week. Pure ethyl acetate also afforded such crystals.

LON-ISO co-crystal: LON (160.58 mg, 0.5 mmol) and ISO (61.06 mg, 0.5 mmol) were dissolved in ethyl acetate (4 mL) at 50 °C then left at ambient conditions for evaporation of solvent to occur. After a week, large colourless block crystals of the 1:1 co-crystal formed.

LON-NICO co-crystal: LON (160.58 mg, 0.5 mmol) and NICO (61.06 mg, 0.5 mmol) were dissolved in an acetonitrile-ethanol solvent mix (80:20 ratio) at 50 °C then left for the solvent to evaporate under ambient conditions. Small colourless plates of the 1:1 co-crystal formed after 2 weeks.

LON-BENZ co-crystal: LON (160.58 mg, 0.5 mmol) and BENZ (60.57 mg, 0.5 mmol) were dissolved in a 50:50 solvent

This journal is © The Royal Society of Chemistry 20xx

Please do not adjust margins

Please do not adjust margins

mix of ethyl acetate and acetonitrile at 50 °C. The solution was left at ambient conditions for solvent evaporation which resulted in small colourless plate crystals forming of the 1:1 co-crystal after 4 days.

LON-MEL salt: LON (160.58 mg, 0.5 mmol) and MEL (63.06 mg, 0.5 mmol) were dissolved in DMSO at 50 °C and left to evaporate at ambient conditions. Initially a gel formed however with extended time (2 weeks to a month) crystals of the 1:1 salt formed in the gel.

LON-PIPE salt: LON (160.58 mg, 0.5 mmol) and PIPE (34.03 mg, 0.05 mmol) were dissolved in 50:50 solvent mix methanol-acetonitrile and left to evaporate under ambient conditions. Large colourless plate crystals of the 1:1 salt formed after 5 days.

LON-HALO salt: LON (160.58 mg, 0.5 mmol) and HALO (187.95 mg, 0.5 mmol) were dissolved in DMF at 50 °C then left under ambient conditions for solvent evaporation to occur. Clusters of colourless plate crystals of the 1:1 salt formed after 6-8 weeks.

LON-IMID salts/co-crystal salts: LON (160.58 mg, 0.5 mmol) and IMID (34.03 mg, 0.5 mmol) were dissolved in ethyl acetate at 50 °C before being left under ambient conditions for solvent evaporation to occur. Colourless block crystals of the 1:1:0.5 salt solvate formed within one day. Crystals of the 2:1 and 1:1 salts were afforded in the same way (from a 1:1 ratio) using a methanol-acetonitrile solvent mix and were observed in the same batch (2:1 ratio material characterised first, 1:1 after some time).

Single crystal X-ray diffraction. Data for LON-NICO, LON-BENZ, LON-4,4BIPY co-crystals and 1:1 LON-IMID salt were collected on a Rigaku FRE+ equipped with VHF Varimax confocal mirrors, an AFC10 goniometer and an HG Saturn724+ detector using Mo-Kα radiation (λ = 0.71075 Å). Crystal Clear 3.1[50,49] software was used for data collection and CrysAlisPro[51,10] for data reduction and Gaussian absorption correction. Data for the remaining samples were collected on an Agilent Technologies Dual Source Supernova, four-circle diffractometer fitted with CCD detector and graphite monochromator using Mo-Kα radiation (λ = 0.71073 Å). CrysAlisPro software was used for data collection, reduction and absorption correction using face indexing and Gaussian corrections. All data was collected at 100K and suitable crystals selected and mounted using paratone or fomblin oil on a MiTeGen Micromesh holder. Structure solution for all was carried out using Direct Methods in SHELXT[52,1] and refined using full-matrix least squares on F2 using SHELXL 2014[53,2] both implemented in the Olex2 software.[54,3] Non-hydrogen atoms were refined with anisotropic displacement parameters. Hydrogen atoms for heteroatoms (N and O) were located from the difference Fourier map, except for one proton in the 2:1 imidazole structure which was set at standard position riding on the parent atom, and all were freely refined. The remaining protons, including those of water molecules in hydrate structures and partially occupied hydrogens in, for example 1:1 imidazole salt were fixed in idealised positions with their displacement parameters riding on the values of their parent atoms.

Various restraints and constraints were used in the structures of LON-IMID 1:1:0.5 ethyl acetate salt solvate and LON-IMID 1:1 salt to give the optimum structure refinement. PLATON,[55,4] with neutron normalised hydrogen bond lengths (for O-H, N-H and C-H at 0.983 Å, 1.009 Å and 1.008 Å respectively), was used for the calculation of bond lengths, bond angles and torsion angles. All cell parameters and refinement information can be seen in Supplementary Information section 5, along with hydrogen bonding tables.

CCDC (1531947-1531963) contain the supplementary crystallographic data for this paper and can be obtained from The Cambridge Crystallographic Data Centre via http://www.ccdc.cam.ac.uk/conts/retrieving.html.

Sample Preparation for Properties Testing. Synthesis of the bulk for all materials was carried out using solvent drop grinding (as per screening method with larger quantities) for LON-NICO, LON-ISO, LON-BENZ and LON-MEL and using the relevant aforementioned solution techniques for LON-IMID, LON-HALO and LON-PIPE. These bulk materials were used for all property measurements and experiments discussed below.

Powder X-ray diffraction (PXRD). For samples generated through grinding screening experiments, for stability and from slurry experiments, data were collected using a Bruker D8 Advance powder X-ray diffractometer with Cu-Kα radiation (λ = 1.54060 Å), with 35 kV and 40 mA voltage and current applied. The sample was scanned from 2θ = 5° to 50° with continuous scan, and a scan rate of 5° min-1. OriginPro 9.1 was used to plot the PXRD patterns obtained.

Differential Scanning Calorimetry (DSC). A TA Instruments Discovery DSC fitted with autosampler and liquid nitrogen pump (LN2P) cooling system was used to measure the thermal behaviour of all samples. Dried samples (free from residual solvent), of mass 2-5 mg, were placed in an aluminium pan (internal volume 20 µL) and crimp sealed with corresponding lid in a Tzero sample press. The heating range was set as 25 °C to 200-300 °C (sample dependent), with a heating rate of 10 °C min^{-1} and nitrogen gas used for purging (base purge 300 mL min^{-1}, cell flow 25 mL min^{-1}).

High Performance Liquid Chromatography (HPLC). HPLC analysis was carried out to quantitatively determine LON concentrations by using a HP 1100 pump fitted G1315B (Agilent Technologies) diode array detector. The LC column was an Agilent Zorbax Eclipse XDB-C18 4.6 x 250 mm, 5µm run at 37 °C. The mobile phase consisted of 25 mM $NaH_2PO_4.H_2O$ (pH 3) and MeOH (30:70 v/v) which was filtered through a 45 µm cellulose filter membrane under vacuum and then sonicated. The mobile phase was pumped isocratically at a flow rate of 1 $mLmin^{-1}$, 20 minute run time. An injection volume of 20 µL was used and detection for all analytes completed at 275 nm. Retention times were: LON 11.85 min, BENZ 2.55 min, HALO 3.14 min, IMID 2.25 min and 2.55 min, ISO 2.5 min, MEL 2.3 min, 2.5 min and 3.2 min, NICO 2.5 min and PIPE 3.36 min. This method was adapted from the work by Ioele et al.[56,5]

Stability Studies. Stability was tested under accelerated conditions (40 °C and 75 % RH) for 13 weeks. Samples of approximately 100 mg size were stored under the test conditions and tested periodically using PXRD to identify the sample's identity.

For slurry experiments, excess co-crystal or salt material in 1 % Tween80® aqueous solution, were left stirring at room temperature for 24 hours before filtering and the resulting powder analysed by PXRD. Solubility of the samples was conducted by taking aliquots of the filtered slurry solution and analysed by HPLC.

Dissolution. Dissolution was tested using an Agilent 708-DS dissolution sampling apparatus with rotation speed of 75 rpm

This journal is © The Royal Society of Chemistry 20xx

Please do not adjust margins

Please do not adjust margins

at 37 °C. 1 % Tween 80® in water dissolution medium (900 mL) was used with samples prepared containing 25 mg API in a 250 mg corn starch tablet, pressed for 1 minute at 2 KN using an FT-IR press. Sampling was conducted by withdrawing 2 mL of sample from the vessel with immediate replacement with fresh dissolution medium to maintain the dissolution volume. 1 mL of the withdrawn sample was discarded as waste, the remainder filtered through a 45 µm syringe tip filter and the sample taken for analysis by HPLC. This was conducted at 5 minute intervals for the first 30 minutes followed by 15 minutes for 30 minutes, a 120 minute sample taken and then hourly sampling until the end of the experiment.

Solubility. Apparent solubility of the unstable materials, LON-ISO, LON-NICO and LON-IMID was calculated according to the literature,[47,48] using the following apparent solubility equation:

$$C_m = C_s \left(\frac{J_m}{J_s}\right)$$

where C_m represents the apparent solubility of the unstable form, C_s represents the solubility of the thermodynamic form, and J_m and J_s represent the dissolution rates of the co-crystal/salt and thermodynamic form, respectively. Linear portions of the dissolution curves of LON and the new materials were used to extract the dissolution rates for the required species.

Dynamic Vapour Sorption (DVS). DVS analysis was carried out on a Surface Measurement Systems DVS Advantage machine. A preheating stage, raising the temperature to 40 °C and holding isothermally for 5 hours, was followed by increasing the partial pressure at 0.2 % per minute from 0-90 % RH and back to 0% in a similar manner via desorption. The system was considered to be in equilibrium if the rate change of mass was less than 0.002 % min^{-1} at one specific partial vapour pressure. The temperature was maintained at a constant 25 °C throughout the experiment. The sorption isotherms were calculated from the equilibrium mass values.

Acknowledgements

This work was funded by the Science and Engineering Research Council of A*STAR. Lucy Mapp would like to thank A*STAR for funding under the A*STAR Research Attachment Programme (ARAP) jointly with The University of Southampton.

References

1. G. P. Stahly, *Cryst. Growth Des.*, 2009, **9**, 4212-4229.
2. N. Shan and M. J. Zaworotko, *Drug Discovery Today*, 2008, **13**, 440-446.
3. C. B. Aakeroy and D. J. Salmon, *CrystEngComm*, 2005, **7**, 439-448.
4. L. Zhou, S. Dodd, C. Capacci-Daniel, S. Garad, R. Panicucci and V. Sethuraman, *Eur. J. Pharm. Sci.*, 2016, **88**, 191-201.
5. B. R. Bhogala and A. Nangia, *New J. Chem.*, 2008, **32**, 800-807.
6. D. P. Elder, R. Holm and H. L. Diego, *Int. J. Pharm.*, 2013, **453**, 88-100.
7. E. Grothe, H. Meekes, E. Vlieg, J. H. ter Horst and R. de Gelder, Cryst. Growth Des., 2016, 16, 3237–3243.
8. N. K. Duggirala, M. L. Perry, Ö. Almarsson and M. J. Zaworotko, Chem. Commun., 2016, 52, 640-655.
9. J. W. Steed, Trends Pharmacol. Sci., 2013, 34, 185-193.
10. N. Blagden, S. J. Coles and D. J. Berry, *CrystEngComm*, 2014, **16**, 5753-5761.
11. H. G. Brittain, *J. Pharm. Sci.*, 2013, **102**, 311-317.
12. US-FDA Select Committee on GRAS Substances (SCOGS) Database, 2013, available at http://www.accessdata.fda.gov/scripts/fdcc/?set=SCOGS
13. US-FDA, Everything added to food in the United States (EUFAS) list of chemicals published by the US-FDA., http://www.accessdata.fda.gov/scripts/fcn/fcnnavigation.cfm?rpt=eafuslisting, (accessed 21/4/16).
14. D. J. Good and N. r. Rodríguez-Hornedo, *Cryst. Growth Des.*, 2009, **9**, 2252-2264.
15. G. L. Perlovich and A. N. Manin, *Russ. J. Gen. Chem.*, 2014, **84**, 407-414.
16. T. Patole and A. Deshpande, *Int. J. Pharm. Sci. Res.*, 2014, **5**, 3566.
17. C. B. Aakeröy, T. K. Wijethunga and J. Desper, *Chem. Eur. J.*, 2015, **21**, 11029-11037.
18. Y. Gao, H. Zu and J. Zhang, *J. Pharm. Pharmacol.*, 2011, **63**, 483-490.
19. V. R. Vangala, P. S. Chow and R. B. H. Tan, *CrystEngComm*, 2011, **13**, 759-762.
20. D. P. McNamara, S. L. Childs, J. Giordano, A. Iarriccio, J. Cassidy, M. S. Shet, R. Mannion, E. O'Donnell and A. Park, *Pharm. Res.*, 2006, **23**, 1888-1897.
21. S. Karki, T. Friščić, L. Fábián, P. R. Laity, G. M. Day and W. Jones, *Adv. Mater.*, 2009, **21**, 3905-3909.
22. L. Ravagnan, I. Marzo, P. Costantini, S. A. Susin, N. Zamzami, P. X. Petit, F. Hirsch, M. Goulbern, M.-F. Poupon and L. Miccoli, *Oncogene*, 1999, **18**, 2537-2546.
23. D. Del Bufalo, D. Trisciuoglio, M. Scarsella, G. D'Amati, A. Candiloro, A. Iervolino, C. Leonetti and G. Zupi, *Neoplasia*, 2004, **6**, 513-522.
24. Lonidamine: Angelini's anticancer agent has been approved for marketing in Italy. *InPharma*, 2013, **583**, 19.
25. P. Ditonno, M. Battaglia, O. Selvaggio, L. Garofalo, V. Lorusso and F. P. Selvaggi, *Rev. Urol.*, 2005, **7**, S27-S33.
26. L. Miccoli, F. Poirson-Bichat, F. Sureau, R. B. Gonçalves, Y. Bourgeois, B. Dutrillaux, M.-F. Poupon and S. Oudard, *J. Ntl. Cancer Inst.*, 1998, **90**, 1400-1406.
27. M. De Cesare, G. Pratesi, A. Giusti, D. Polizzi and F. Zunino, *Br. J. Cancer*, 1998, **77**, 434.
28. L. Milane, Z. Duan and M. Amiji, *PLoS ONE*, 2011, **6**, e24075.
29. M. K. Brawer, *Rev. Urol.*, 2005, **7**, S21-S26.
30. S. Marrache and S. Dhar, *Proceedings of the National Academy of Sciences of the United States of America*, 2012, **109**, 16288-16293.
31. F. Benetollo, A. Pra, F. Orsini and L. Baiocchi, *J. Crystallogr. Spectrosc. Res.*, 1993, **23**, 987-992.
32. J. Xinmin, W. Xiaoqi, G. Wu and Z Weibin, Crystalline Form I of Lonidamine, Preparation Method Thereof and Composite Containing The Same, CN 101735151 B, 2012.
33. G. R. Desiraju, *Angew. Chem., Int. Ed.*. 1995, **34**, 2311-2327.
34. I. J. Bruno, J. C. Cole, P. R. Edgington, M. Kessler, C. F. Macrae, P. McCabe, J. Pearson and R. Taylor, *Acta Crystallogr. Sect. B*, 2002, **58**, 389-397.

Formatted: English (United Kingdom)

Formatted: English (United Kingdom)

Formatted: Indent: Left: 0 cm, First line: 0 cm

Formatted: English (United Kingdom)

Please do not adjust margins

Please do not adjust margins

54. C. F. Macrae, P. R. Edgington, P. McCabe, E. Pidcock, G. P. Shields, R. Taylor, M. Towler and J. van de Streek, *J. Appl. Crystallogr.*, 2006, **39**, 453-457.
65. C. F. Macrae, I. J. Bruno, J. A. Chisholm, P. R. Edgington, P. McCabe, E. Pidcock, L. Rodriguez-Monge, R. Taylor, J. van de Streek and P. A. Wood, *J. Appl. Crystallogr.*, 2008, **41**, 466-470.
76. M. C. Etter, *Acc. Chem. Res.*, 1990, **23**, 120-126.
87. P. H. Stahl and C. G. Wermuth, *Ed. Handbook of Pharmaceutical Salts: Properties, Selection, and Use; International Union of Pure and Applied Chemistry*, Wiley-VCH, Weinheim, NY; USA, 2002.
98. A. J. Cruz-Cabeza, *CrystEngComm*, 2012, **14**, 6362-6365.
3940. M. L. Cheney, N. Shan, E. R. Healey, M. Hanna, L. Wojtas, M. J. Zaworotko, V. Sava, S. Song and J. R. Sanchez-Ramos, *Cryst. Growth Des.*, 2009, **10**, 394-405.
410. M. L. Cheney, D. R. Weyna, N. Shan, M. Hanna, L. Wojtas and M. J. Zaworotko, *Cryst. Growth Des.*, 2010, **10**, 4401-4413.
421. A. Delori and W. Jones, *CrystEngComm*, 2011, **13**, 6315-6318.
432. J. Szegezdi and F. Csizmadia, presented in part at the American Chemical Society Spring Meeting, March 25-29th, Chicago, Illinois, USA, 25-29th March 2007, 2007.
443. ChemAxon, *MarvinSketch 16.4.25*, 2016. (http://www.chemaxon.com).
454. S. L. Childs, G. P. Stahly and A. Park, *Mol. Pharmaceut.*, 2007, **4**, 323-338.
465. C. B. Aakeroy, S. Forbes and J. Desper, *Journal of the American Chemical Society*, 2009, **131**, 17048-17049.
476. M. K. Stanton and A. Bak, *Cryst. Growth Des.*, 2008, **8**, 3856-3862.
487. J. H. Fagerberg, O. Tsinman, N. Sun, K. Tsinman, A. Avdeef and C. A. S. Bergström, *Mol. Pharmaceut.*, 2010, **7**, 1419-1430.
498. P. Sanphui, N. R. Goud, U. B. R. Khandavilli and A. Nangia, *Cryst. Growth Des.*, 2011, **11**, 4135-4145.
5049. Rigaku, *CrystalClear-SM Expert 3.1 b27*, 2013.
510. *CrysalisPro*, Agilent Technologies: Oxfordshire, 2013.
521. G. Sheldrick, *Acta Crystallogr., Sect. A: Found. Adv.*, 2015, **71**, 3-8.
532. G. M. Sheldrick, *Acta Crystallogr.*, 2008, **A64**, 112-122.
543. O. V. Dolomanov, L. J. Bourhis, R. J. Gildea, J. A. K. Howard and H. Puschmann, *J. Appl. Crystallogr.*, 2009, **42**, 339-341.
554. A. Spek, *Acta Cryst.*, 2009, **D65**, 148-155.
565. G. Ioele, M. De Luca and G. Ragno, *Anal. Methods*, 2013, **5**, 1715.

Table of contents entry

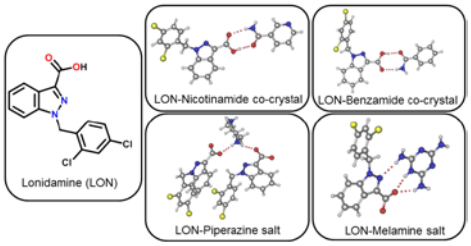

Novel co-crystal and salt forms of an anticancer drug, lonidamine (LON), were identified and characterised by thermal and X-ray diffraction techniques. Evaluation of physicochemical properties revealed that the co-formers were able to modulate the properties of LON.

This journal is © The Royal Society of Chemistry 20xx

Please do not adjust margins